Applied Physics Letters

Acoustic energy harvesting based on multilateral metasurfaces

Cite as: Appl. Phys. Lett. **111**, 243506 (2017); https://doi.org/10.1063/1.5003299
Submitted: 05 September 2017 • Accepted: 29 November 2017 • Published Online: 13 December 2017

Shuibao Qi and Badreddine Assouar

Acoustic energy harvesting based on multilateral metasurfaces

Shuibao Qi[1,2] and Badreddine Assouar[1,2,a)]
[1]CNRS, Institut Jean Lamour, Vandœuvre-lès-Nancy F-54506, France
[2]Université de Lorraine, Institut Jean Lamour, Boulevard des Aiguillettes, BP: 70239, Vandœuvre-lès-Nancy 54506, France

(Received 5 September 2017; accepted 29 November 2017; published online 13 December 2017)

We theoretically and numerically report on an innovative acoustic energy harvester based on acoustic multilateral metasurfaces and a piezoelectric bimorph. The coiling-up-space concept realized by labyrinthine units is applied to achieve the desired phase profiles for the acoustic focusing and energy confinement. The acoustic energy confined by the metasurfaces from a point source is converted into electrical energy by a structured piezoelectric bimorph. Numerical simulations and theoretical analysis evidenced that the output voltage and power drastically increase with the sides of the multilateral metasurface energy harvesting system. Maximum output voltage and power 52 and 407 times higher than those under the case without metasurfaces are achieved with enclosed multilateral metasurface design. *Published by AIP Publishing*. https://doi.org/10.1063/1.5003299

With the advances in micro/nano-electronic devices and novel materials, acoustic energy has aroused increasing interest of scientists and engineers due to its clean, renewable, and abundant properties. Generally, acoustic energy harvesting (AEH) is to confine or localize the sound/noise from various ambient environments and convert it into electric energy. Many scientific and engineering efforts have been endeavored to improve the AEH efficiency and performance from the aspects of sound scavenging[1–4] and energy converting[5–8] as well. Due to low power density, a Helmholtz resonator configured with a piezoelectric composite diaphragm on the bottom[5] was intuitively applied to construct an electromechanical Helmholtz resonator (EMHR) for AEH, and a maximum power density of 0.34 μW/cm^3 was acquired with an input sound pressure level (SPL) of 149 dB. Liu *et al.*[1] extended the AEH system based on EMHR to achieve an output power of 30 mW with an input SPL of 160 dB. A quarter wavelength straight tube resonator with an array of piezoelectric cantilevers inside was designed for AEH,[2] and the work frequency heavily depends on the geometrics of the tube. In general, the mostly applied AEH methodology based on Helmholtz resonators or other chamber resonators[9] suffers from the defects of the bulky system, uncontrollable sound field, and lack of spatial flexibility, which hamper and restrict the application scope of acoustic energy as a power source.

Unlike the traditional acoustic cavity resonators confining the sound waves within the cavity, the artificially engineered acoustic metamaterials[10–12] emerging recently possess anomalous properties and advantageous capabilities in various kinds of sound wave manipulations,[13–17] which provide more degrees of freedom for the flexible and practical AEH in broad applications. As a group of planar metastructures with the additional advantage of ultrathin (subwavelength) thickness features, acoustic metasurfaces (AMs) share the capability of acoustic metamaterials in reflected, refracted, and transmitted sound wave manipulations, such as diffusion,[18] unidirectional transmission,[19] lensing,[13,20] and absorption.[21] Wavefront manipulations with AMs are dominated by the phase control of the reflected or transmitted waves. Inspired by the generalized Snell law initiated in the field of optics,[22] the coiling up space concept has been used to realize AMs[23–25] for a predefined phase profile for desired wave tailoring. Because of the fully controllable wave field and the planar features, the partially or enclosed multilateral AMs catching more impinging sound waves from a point source, together with a piezoelectric bimorph energy converter, are unprecedentedly applied in this paper for effective and efficient AEH. Instead of confining the acoustic energy into the whole metamaterial cavity,[26] the idea is to arbitrarily focus and confine the acoustic waves from a point sound source by the multilateral AMs at any designed position and subsequently convert the confined acoustic energy into electrical energy through a piezoelectric cantilever bimorph system.

Labyrinthine units are utilized for space coiling in this paper. A typical labyrinthine unit structure with length l_y and width l_x for reflected wave manipulation is illustrated in Fig. 1(a), and the incident and reflected waves are working in horizontal direction x. The rigid identical bars with length l and width w from the upper and lower boundaries are arrayed in parallel with an equal gap d to form a meandering air channel for sufficient reflected wave delay. The labyrinthine unit shown in Fig. 1(a) is configured in $(m, n) = (3, 2)$, where m and n denote the number of bars from the upper and lower beams (thickness t), respectively. The integer variables m and n can be varied and combined to form four groups of labyrinthine configurations, viz., (3, 2), (2, 2), (2, 1), and (1, 1). In order to minimize the thermo-viscous effect, eight labyrinthine units from these four (m, n) configurations are optimized to discretely and completely cover the 2π phase shift with a resolution of $\pi/4$. In order to get a concise wavelength, the work frequency is selected as 3430 Hz for all the numerical simulations and theoretical calculations in this paper. The sound velocity in air is 343 m/s, and thus, the wavelength is $\lambda = 0.1$ m. The length l_y and width l_x of the eight selected units are fixed to be 0.0125 m ($\lambda/8$) to maintain the phase shift resolution and sub-wavelength property. The

a)Author to whom correspondence should be addressed: Badreddine.Assouar@univ-lorraine.fr

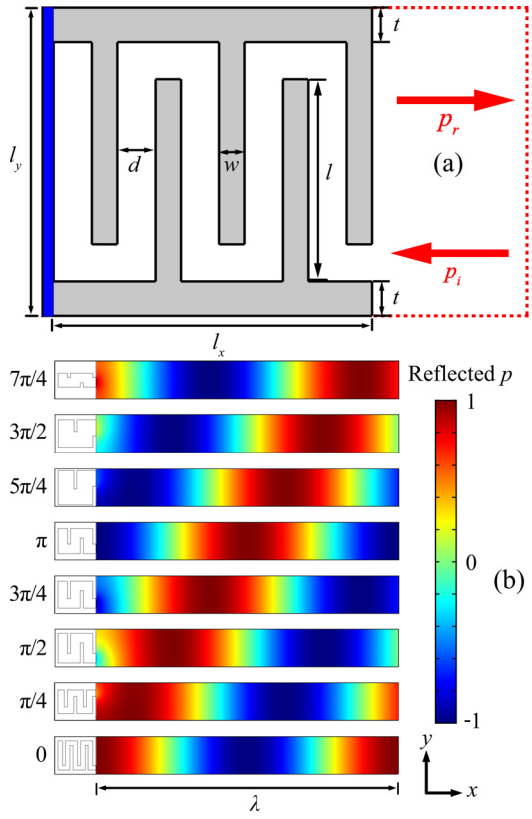

FIG. 1. (a) Sketch of a typical labyrinthine unit (width l_x and length l_y) under the configuration $(m, n) = (3, 2)$. (b) Normalized reflected sound pressure field evolutions of the eight labyrinthine units from four different (m, n) configurations.

width (w) of the bars is set as 1 mm ($\lambda/100$), and the thickness t of the upper and lower bars for the four (m, n) configurations is set within the range (0.5 mm, 5 mm) or ($\lambda/200$, $\lambda/20$).

Through numerical simulation, the phase shift performances of all the eight selected labyrinthine units from (3, 2), (2, 2), (2, 1), and (1, 1) configurations are individually investigated and consistently demonstrated in Fig. 1(b). As shown in Fig. 1(b), the incident waves are impinging from the right ends, and the reflected sound pressure fields with one wavelength (0.1 m) formed by the left labyrinthine units are normalized to each maximum value. Viewing from the bottom to the top of Fig. 1(b), the selected labyrinthine units gradually and completely shift the phase of the reflected waves from the 0 to 2 π range with a fine discrete resolution of $\pi/4$ as designed and desired.

The schematic diagram of an AEH system based on a two-sided multilateral metasurface and a piezoelectric bimorph energy converter is illustrated in Fig. 2(a). The point sound source (x_s, y_s) is placed in the center, and the arbitrarily designed focusing point (x_f, y_f) is in the lower-right corner. The lower and right sides of the AEH system shown in Fig. 2(a) are set as perfectly matched layers (PMLs), and the theoretical phase profiles of the left and upper sides (resembled by the multilateral metasurface) required to achieve the phase contour line (blue arc) for the focusing at (x_f, y_f) can be expressed as

$$\varphi_1(y) = k\left[\sqrt{(y-y_s)^2 + x_s^2} - x_s + \sqrt{(y-y_f)^2 + x_f^2} - x_f\right] \quad (1)$$

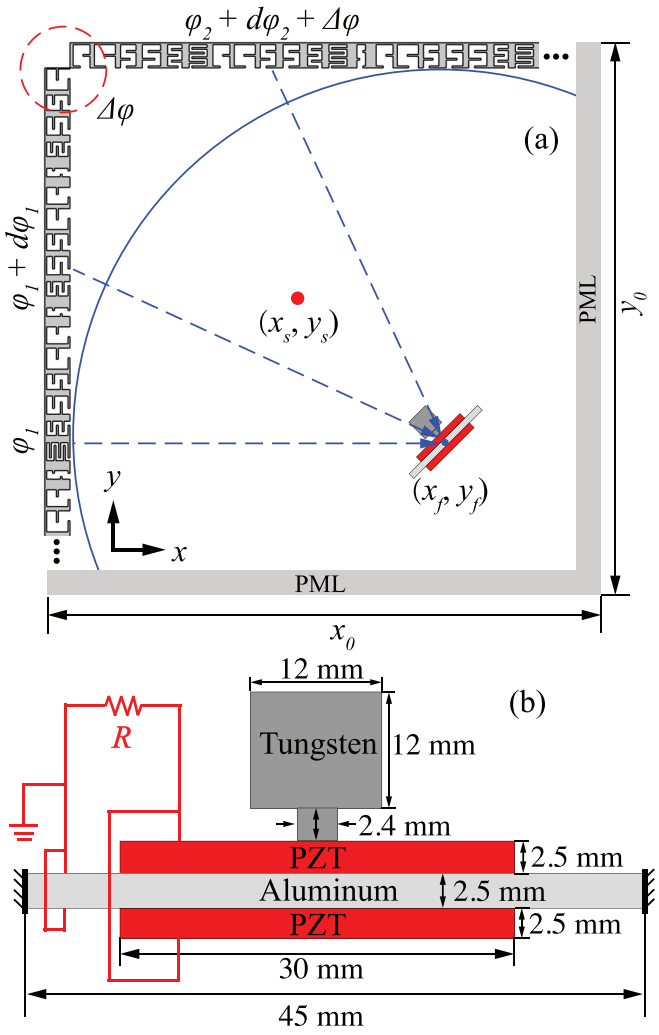

FIG. 2. (a) Schematic diagram of a partially enclosed AEH system composed of two perpendicular metasurfaces and a piezoelectric bimorph cantilever. (b) Sketch of the piezoelectric bimorph acoustic energy converter with a tungsten mass and a resistive load circuit.

and

$$\varphi_2(x) = k\left[\sqrt{(x-x_s)^2 + (y_0-y_s)^2} - (y_0-y_s) + \sqrt{(x_f-x)^2 + (y_0-y_f)^2} - (y_0-y_f) + \Delta\varphi\right], \quad (2)$$

where x_0 and y_0 are the length and width of the system and k and $\Delta\varphi$ are the wave number and additional phase shift, respectively. Considering the phase continuity of the two individual metasurfaces at the joint shown in Fig. 2(a), $\Delta\varphi$ can be expressed as

$$\Delta\varphi = k(2y - x_f - y_f - x_s - y_s). \quad (3)$$

The size of the system (x_0, y_0) is set to be (1 m, 1 m) or $(10\lambda, 10\lambda)$, and thus, 80 elementary labyrinthine units from the eight types shown in Fig. 1(b) are arrayed in the left and upper sides to construct the multilateral metasurface to discretely fit the theoretical phase profile required for the designed focusing at (x_f, y_f). It is worth noting that the size of

the system can be varied as required for various applications, and the system can be still effective until its size going down to $(3\lambda, 3\lambda)$ or 3λ for the one-sided case.

Because of high energy conversion efficiency and smaller size at a given resonance frequency, the piezoelectric (PZT-5 H) bimorph cantilever with a tip mass[27] is selected and placed in the focusing region of Fig. 2(a) to convert the confined acoustic energy into electrical energy. As schematically demonstrated in Fig. 2(b), two identical PZT plates with length 30 mm and thickness 2.5 mm are symmetrically attached to a both-end-clamped shim with length 45 mm and thickness 2.5 mm to construct the PZT bimorph cantilever. A stepped square tungsten block with length 12 mm is deposited in the middle of the cantilever to work as a tip mass. The minimum size of the confined spot formed by the AMs is slightly larger than the diffraction limit of 50 mm (0.5 λ). Therefore, the dimension of the PZT bimorph cantilever is optimized to be 45 mm by 22 mm, balanced to be large enough to sufficiently catch the confined energy yet small enough to avoid the influence of effectiveness of the acoustic energy confinement. The geometrical parameters of the PZT converter are also carefully tuned to ensure that the fundamental resonating frequency of the system matches the work frequency of the AMs, viz., 3430 Hz. The PZT plates only cover the middle part of the aluminum shim to avoid the charge canceling effect,[28] and the tip mass on the top is stepped to minimize its coverage area (zero strain area) on the PZT plate. The two PZT plates are connected in series[29] to form an electrical circuit with resistive load. Rigorous and detailed studies on the PZT bimorph cantilevers can be found in the literatures.[27,30]

Commercial finite element analysis (FEA) software COMSOL Multiphysics^{TM} Version 5.2a is utilized to analyze and simulate the labyrinthine unit in Fig. 1 and the AEH system shown in Fig. 2. Pressure acoustics, solid mechanics, and electrostatics modules are applied for the coupling of the acoustic, mechanical, and electrostatic fields, and the resistive load circuit is simulated by the electrical circuit module. The density and Young's modulus of the aluminum plate and tungsten mass for computation are 2700 and 17 800 kg/m^3 and 3.6×10^5 and 7×10^4 MPa, respectively. The mechanical damping coefficient of the PZT bimorph system is set as 0.015 for the calculation. As the input parameters, the positions of the point sound source and the focusing are arbitrarily set at (0.5 m, 0.5 m) and (0.75 m, 0.16 m), respectively. In this case, the numerically and theoretically acquired results from the AEH system and the theoretical designs are demonstrated in Fig. 3. The numerical result

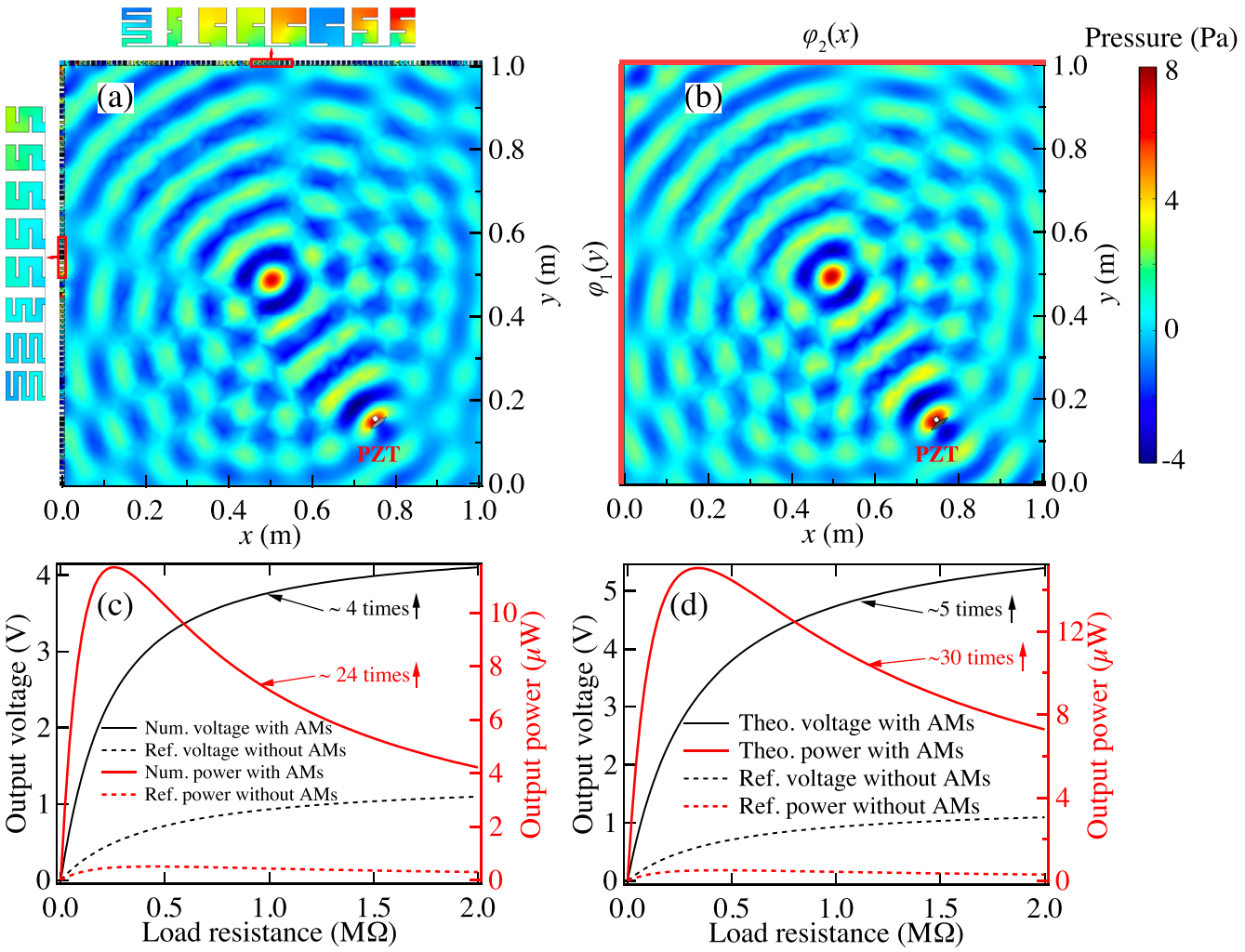

FIG. 3. (a) Numerical sound pressure field formed by the two-sided multilateral metasurface. (b) Sound pressure field formed by the theoretically designed phase profiles. (c) and (d) The output voltage and power of the multilateral metasurface and theoretical designs, respectively.

shown in Fig. 3(a) is obtained through the simulation of the interaction of the metasurface structure and incident waves, and the theoretical result illustrated in Fig. 3(b) is acquired through the phase profile analysis in the corresponding boundaries. As illustrated in Fig. 3(a), the sound waves reflected from the metasurface walls are well focused in the designed focusing position (0.75 m, 0.16 m) where the PZT bimorph is positioned. Even though there are some fluctuations in each wave front line caused by the slight phase discontinuity, obvious focusing wave fronts around the designed focusing position (0.75 m, 0.16 m) can be readily observed in Fig. 3(a), and the specific sound pressure distributions in the sampled labyrinthine units are amplified and demonstrated in the left an upper sides. Theoretical designs with impedance boundaries for desired phase profiles on the sides/frames are highlighted in red in Fig. 3(b), and a similar and perfect focusing pattern at (0.75 m, 0.16 m) is observed. Because the focusing region is small and the PZT bimorph system shown in Fig. 2(b) presents narrow directivity properties, the specific position and the angle of the PZT bimorph are sufficiently and carefully swept to maximize the output voltage and power. The electrical outputs from numerical and theoretical AEH systems are demonstrated in Figs. 3(c) and 3(d), respectively. The referenced output voltages (see dashed black lines) and powers (see dashed red lines) shown in Figs. 3(c) and 3(d) are obtained from the same PZT cantilever bimorph at the same position (0.75 m, 0.16 m) in the free sound field without AMs or theoretical designs in the boundaries. The volume flow rate out from the point sound source is set to be 5×10^{-4} m^2/s for all the cases. As demonstrated in Fig. 3(c), the output voltage evolution curve (see black solid line) increases with the load resistance until reaching saturation, while the output power (see red solid line) increases with the load resistance to a peak and then decreases. The same trends can be observed in theoretical results shown in Fig. 3(d). The maximum output voltages can reach 4 and 5 V for numerical and theoretical cases, which are about 4 and 5 times of the referenced voltages, respectively. The maximum output powers are 12 μW and 15 μW for numerical and theoretical cases, which are about 24 and 30 times of the referenced powers, respectively. The small difference between the numerical and theoretical output results can be explained by the phase discontinuity and a small amount of energy retained within the labyrinthine cavities.

Figure 3 provides one specific example of AEH with two-sided AMs and the structured PZT bimorph converter. The AM configurations can be extended to three and four sided cases. For better comparison, the AEH system with a one-sided metasurface is also calculated, and all the maximum output powers and voltages for the corresponding configurations are obtained and demonstrated in Fig. 4. As can be seen in Fig. 4, the maximum output voltage V_{max} (solid black line with squares) and power P_{max} (solid red line with circles) ratios with AMs to those without (the dashed black line with squares V_{ref} and the dashed red line with circles P_{ref}) increase with the number of sides of the AEH system. The maximum electrical outputs are achieved in the case of the four-sided multilateral AEH system, and the output

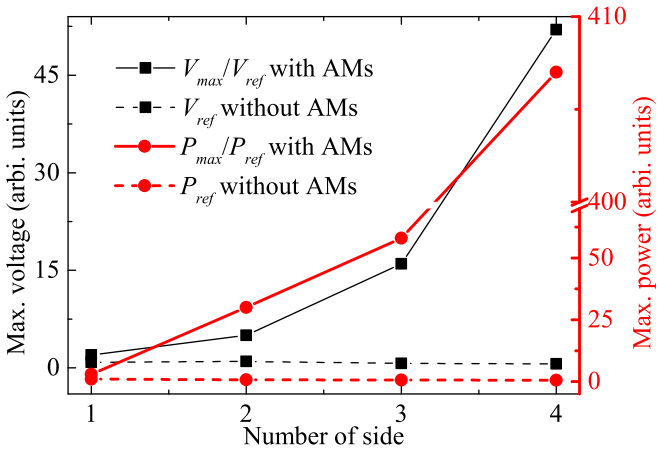

FIG. 4. Amplified and intensified output voltage and power from the AEH system with the increasing degree of enclosure from one to four sides.

voltage and power are 52 and 407 times higher than those without AMs, respectively.

In summary, based on generalized Snell's law and the coiling-up-space concept in the scope of acoustics, multilateral metasurfaces with a structured PZT bimorph acoustic energy converter are applied to construct an innovative AEH system with the features of full flexibility, easy fabrication, and broad applications. The output voltage and power increase with enclosure degrees of the AEH system. Due to its easy fabrication and fully controllable in spatial dimension, the proposed AEH system based on multilateral AMs and piezoelectric bimorph converter should be readily applicable for microenergy production and ideally work as a power source for public or private micro/nano-devices in a large variety of partially or completely enclosed space environments.

This work was supported by "la Région du Grand Est" and the project "MASS" funded by ICEEL - CARNOT.

[1]F. Liu, A. Phipps, S. Horowitz, K. Ngo, L. Cattafesta, T. Nishida, and M. Sheplak, J. Acoust. Soc. Am. **123**, 1983 (2008).
[2]B. Li, J. H. You, and Y. J. Kim, Smart Mater. Struct. **22**, 055013 (2013).
[3]L. Y. Wu, L. W. Chen, and C. M. Liu, Appl. Phys. Lett. **95**, 013506 (2009).
[4]S. Qi, M. Oudich, Y. Li, and B. Assouar, Appl. Phys. Lett. **108**, 263501 (2016).
[5]S. B. Horowitz, M. Sheplak, L. N. Cattafesta, and T. Nishida, J. Micromech. Microeng. **16**, S174 (2006).
[6]M. Lallart, D. Guyomar, C. Richard, and L. Petit, J. Acoust. Soc. Am. **128**, 2739 (2010).
[7]A. F. Arrieta, P. Hagedorn, A. Erturk, and D. J. Inman, Appl. Phys. Lett. **97**, 104102 (2010).
[8]G. Scarselli, F. Nicassio, F. Pinto, F. Ciampa, O. Iervolino, and M. Meo, Smart Mater. Struct. **25**, 055001 (2016).
[9]F. U. Khan and Izhar. J. Micromech. Microeng. **25**, 023001 (2015).
[10]Z. Liu, X. Zhang, Y. Mao, Y. Y. Zhu, Z. Yang, C. T. Chan, and P. Sheng, Science **289**, 1734 (2000).
[11]J. Li and C. T. Chan, Phys. Rev. E **70**, 021205 (2004).
[12]N. Fang, D. Xi, J. Xu, M. Ambati, W. Srituravanich, C. Sun, and X. Zhang, Nat. Mater. **5**, 452 (2006).
[13]J. Christensen and F. J. de Abajo, Phys. Rev. Lett. **108**, 124301 (2012).
[14]J. Zhu, J. Christensen, J. Jung, L. Martin-Moreno, X. Yin, L. Fok, X. Zhang, and F. J. Garcia-Vidal, Nat. Phys. **7**, 52 (2011).
[15]M. H. Lu, X. K. Liu, L. Feng, J. Li, C. P. Huang, Y. F. Chen, Y. Y. Zhu, S. N. Zhu, and N. B. Ming, Phys. Rev. Lett. **99**, 174301 (2007).
[16]B. Liang, X. S. Guo, J. Tu, D. Zhang, and J. C. Cheng, Nat. Mater. **9**, 989 (2010).

[17]M. Oudich, M. B. Assouar, and Z. Hou, Appl. Phys. Lett. **97**, 193503 (2010).
[18]Y. Zhu, X. Fan, B. Liang, J. Cheng, and Y. Jing, Phys. Rev. X **7**, 021034 (2017).
[19]Y. Li, B. Liang, X. Y. Zou, and J. C. Cheng, Appl. Phys. Lett. **103**, 063509 (2013).
[20]W. Wang, Y. Xie, A. Konneker, B. I. Popa, and S. A. Cummer, Appl. Phys. Lett. **105**, 101904 (2014).
[21]Y. Li and M. B. Assouar, Appl. Phys. Lett. **108**, 063502 (2016).
[22]N. Yu, P. Genevet, M. A. Kats, F. Aieta, J. P. Tetienne, F. Capasso, and Z. Gaburro, Science **334**, 333 (2011).
[23]S. Qi, Y. Li, and B. Assouar, Phys. Rev. Appl. **7**, 054006 (2017).
[24]Y. Li, X. Jiang, R. Q. Li, B. Liang, X. Y. Zou, L. L. Yin, and J. C. Cheng, Phys. Rev. Appl. **2**, 064002 (2014).
[25]K. Song, J. Kim, S. Hur, J. H. Kwak, S. H. Lee, and T. Kim, Sci. Rep. **6**, 32300 (2016).
[26]K. H. Sun, J. E. Kim, J. Kim, and K. Song, Smart Mater. Struct. **26**, 075011 (2017).
[27]S. Roundy and P. K. Wright, Smart Mater. Struct. **13**, 1131 (2004).
[28]R. Kashyap, T. R. Lenka, and S. Baishya, IEEE Electron Device Lett. **36**, 1369 (2015).
[29]A. Erturk and D. J. Inman, Smart Mater. Struct. **18**, 025009 (2009).
[30]J. Ajitsaria, S. Y. Choe, D. Shen, and D. J. Kim, Smart Mater. Struct. **16**, 447 (2007).